Mass (Heat) Transfer Downstream of Blockages With Round and Elongated Holes in a Rectangular Channel

H. S. Ahn

S. W. Lee

S. C. Lau[1]

D. Banerjee

Convective Heat and Mass Transfer Laboratory,
Department of Mechanical Engineering,
Texas A&M University,
College Station, TX 77843-3123

Turbulent forced convective mass (heat) transfer downstream of blockages with round and elongated holes in a rectangular channel was studied. The blockages and the channel had the same 12:1 (width-to-height ratio) cross section, and a distance equal to twice the channel height separated consecutive blockages. The diameter of the holes was either 0.5 or 0.75 of the height of the channel. Naphthalene sublimation experiments were conducted with four hole aspect ratios (hole-width-to-height ratios) between 1.0 and 3.4, two hole-to-channel area ratios (ratios of total hole cross-sectional area to channel cross-sectional area) of 0.2 and 0.3, and Reynolds numbers (based on the channel hydraulic diameter) of 7000 and 17,000. The effects of the hole aspect ratio, for each hole-to-channel area ratio, on the average mass (heat) transfer and the local mass (heat) transfer distribution on the exposed primary channel wall between consecutive blockages were examined. The results of the study showed that the blockages with holes caused the average mass (heat) transfer to be as high as about eight times that for fully developed turbulent flow through a smooth channel at the same mass flow rate. The elongated holes caused higher overall mass (heat) transfer and larger spanwise variation of the local mass (heat) transfer on the channel wall than round holes. [DOI: 10.1115/1.2767748]

Keywords: forced convection, heat transfer enhancement, turbulent flow, naphthalene sublimation

Introduction

To protect the vanes and the blades in gas turbine engines from the hot combustion gases, air from the compressors is forced to flow through shaped internal cooling passages. The cooling air leaves the airfoils through strategically located film cooling holes on the pressure and suction walls, and at the tips of the airfoils, and through slots along the trailing edges of the airfoils. Along the internal cooling passages, there may be holes for impingement cooling of the airfoil leading edges, which are subjected to very high heat fluxes. There may be turbulators on the surfaces of the straight or serpentine internal cooling channels, and pin fins in the channels near the trailing edges, to enhance the heat transfer to the cooling air. Han et al. [1] presented a comprehensive survey of published experimental and numerical studies of internal cooling of gas turbine airfoils. Other recent studies, such as Refs. [2–8], gave the latest accomplishments of several research groups that have conducted research on internal cooling of gas turbine airfoils.

In a design concept for protecting the trailing edge region of an airfoil, cooling air is forced to flow through two to three blockages with staggered holes, before it exits the airfoil through the trailing edge slots. Each blockage has the same cross section as the flow cross section between the pressure and suction walls. After passing through the holes along a blockage, the cooling air impinges onto the next blockage and is deflected toward the suction and pressure walls of the airfoil before it passes through the staggered holes along the next blockage.

In Ref. [9], the tail region of an airfoil with these blockages was modeled as two converging rectangular channels. Air flowed through elongated holes with rounded edges along two blockages in each channel, after the air made a right-angled turn in an entrance channel. Downstream of the second blockage, the air exited through slots separated by lands with rounded leading edges. Two different entrance channels and two exit slot configurations were considered. Naphthalene sublimation experiments were conducted to determine the overall mass transfer coefficients and the distributions of the local mass transfer coefficient on the walls between the two blockages and between the second blockage and the exit slots. The analogy between heat transfer and mass transfer was used to relate the experimentally determined mass transfer enhancement to heat transfer enhancement.

Moon and Lau [10] conducted experiments with thermochromic liquid crystals to obtain the average heat transfer coefficients and the local heat transfer distributions on one of the channel walls between two blockages with round holes, and the overall pressure drops across the blockages, for nine different staggered configurations of holes in the blockages. Lau et al. [11] conducted naphthalene sublimation experiments to study heat transfer enhancement by blockages with staggered round holes and square holes with rounded corners for turbulent airflows through a wide rectangular channel.

There have been a number of other heat transfer studies on turbulent flows through channels with perforated blockages or blockages with various openings for flows to pass through, such as Kukreja and Lau [12], Hwang et al. [13], Liou and Chen [14], and Buchlin [15]. However, the blockages in these studies had cross sections that were much smaller than the cross sections of the channels such that air flowed over the blockages as well as through the openings in the blockages.

The objective of this study was to examine, for turbulent airflow through holes in blockages, the effects of the aspect ratio (width-to-height ratio) of the holes and the hole-to-channel area ratio on the overall heat transfer and local heat transfer distribu-

[1]Corresponding author.

Contributed by the Heat Transfer Division of ASME for publication in the JOURNAL OF HEAT TRANSFER. Manuscript received June 23, 2006; final manuscript received April 29, 2007. Review conducted by Bengt Sunden.

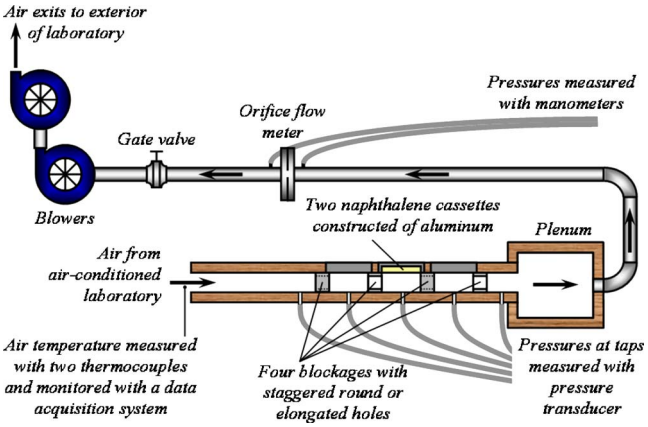

Fig. 1 Schematic of test apparatus for mass transfer experiments (not to scale)

tions on the two principal walls between consecutive blockages, and the pressure drops across the blockages. These blockages were oriented perpendicular to the main flow direction in a wide rectangular channel and had the same cross section as the flow channel. Naphthalene sublimation experiments were conducted to obtain the overall mass transfer and local mass transfer distributions for two flow rates corresponding to Reynolds numbers (based on the channel hydraulic diameter) of 7000 and 17,000. The heat and mass transfer analogy was used to relate the mass transfer enhancement to heat transfer enhancement. This parametric study was different from Lau et al. [9] in which blockages with two specific hole configurations (elongated holes with rounded edges) in two converging rectangular channels with specific dimensions and entrance and exit configurations were considered.

Test Apparatus

The main components of the test apparatus for this study are the test section, a settling chamber, an orifice flow meter, a control valve, and two centrifugal blowers (Fig. 1). The test section is a rectangular channel that has a cross section of 30.5 cm (width) $\times$2.54 cm (height), and thus, an aspect ratio of 12:1. The walls of the test section are constructed of 1.27-cm-thick oak plywood. As shown in the schematic of the top view of the test section with the top wall removed in Fig. 2, there are four blockages with round or elongated holes in the test section. These blockages have the same cross section as the cross section of the test section. They are constructed of acrylic and are 1.14 cm thick, and the distance between consecutive blockages is equal to 5.08 cm, or, two times the height of the channel. Figure 2 also shows that the holes in

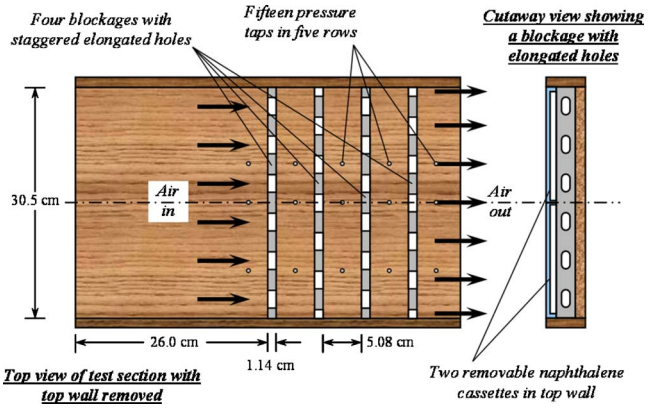

Fig. 2 Schematic of test section showing four blockages with elongated holes and naphthalene cassettes in top wall

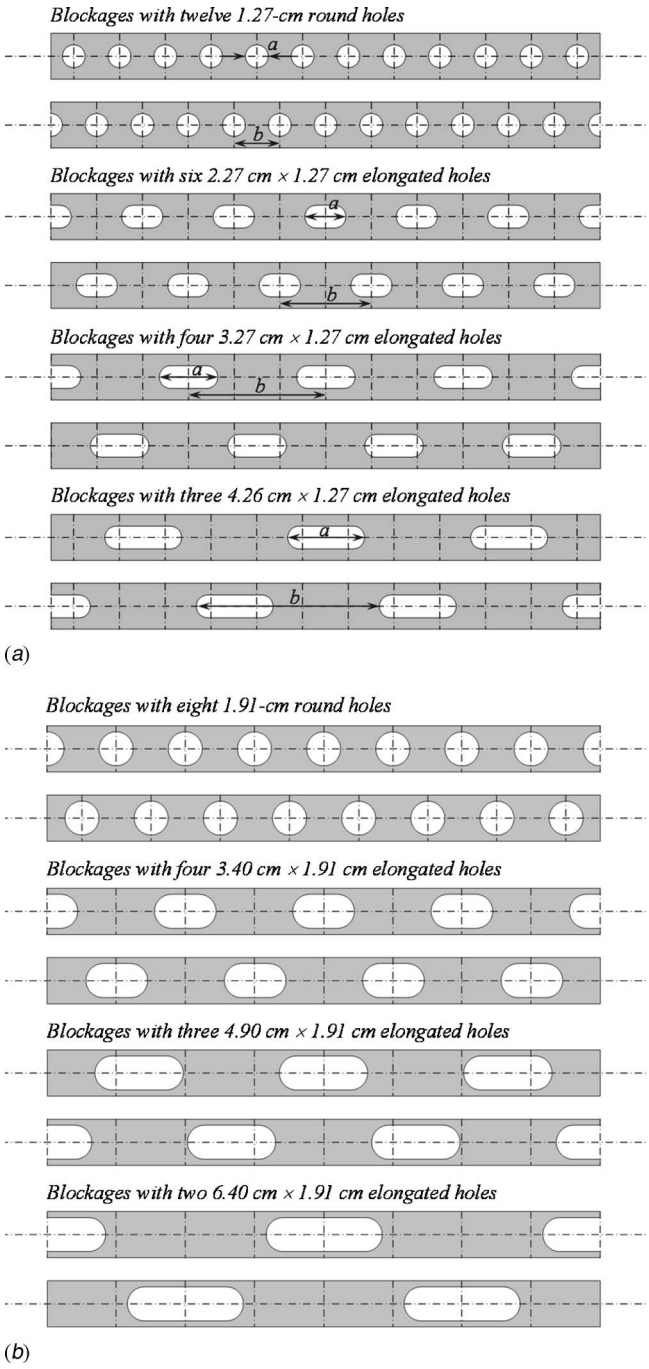

Fig. 3 (*a*) Blockages with round or elongated holes; diameter of holes equals $\frac{1}{2}$ of channel height. (*b*) Blockages with round or elongated holes; diameter of holes equals $\frac{3}{4}$ of channel height.

consecutive blockages are staggered to induce secondary flows, as air passes through the blockages during an experiment, to enhance the mass transfer on the exposed surfaces of the primary walls of the test channel.

For this study, the round or elongated holes in the four blockages have a diameter of either 1.27 cm or 1.91 cm, or, $\frac{1}{2}$ or $\frac{3}{4}$ of the height of the channel. There are eight sets of blockages with different hole configurations. Figures 3(*a*) and 3(*b*) show the blockages with holes that have diameters of 1.27 cm and 1.91 cm, respectively. Table 1 lists the dimensions of the holes and the spacings between holes in the various blockages. While the aspect

Table 1 Dimensions of holes in blockages

Smaller holes, $d=1.27$ cm	Case S-1	Case S-2	Case S-3	Case S-4
Number of holes in each blockage	12	6	4	3
Shape of holes	Round	Elongated	Elongated	Elongated
Width of holes, a	1.27 cm	2.27 cm	3.27 cm	4.26 cm
Center-to-center spacing between holes, b	2.54 cm	5.08 cm	7.62 cm	10.16 cm
Cross-sectional area of each hole	1.27 cm^2	2.53. cm^2	3.80 cm^2	5.07 cm^2
Aspect ratio of holes	1.00	1.79	2.57	3.36
Total hole-to-channel area ratio	0.196	0.196	0.196	0.196
Larger holes, $d=1.91$ cm	Case L-1	Case L-2	Case L-3	Case L-4
Number of holes in each blockage	8	4	3	2
Shape of holes	Round	Elongated	Elongated	Elongated
Width of holes, a	1.91 cm	3.40 cm	4.90 cm	6.40 cm
Center-to-center spacing between holes, b	3.81 cm	7.62 cm	10.66 cm	15.24 cm
Cross-sectional area of each hole	2.85 cm^2	5.70 cm^2	8.55 cm^2	11.40 cm^2
Aspect ratio of holes	1.00	1.79	2.57	3.36
Total hole-to-channel area ratio	0.295	0.295	0.295	0.295

ratio of the holes ranges from 1.00 (round holes) to 3.36, and the total number of holes varies from 2 to 12, the ratios of the total hole-to-channel cross-sectional areas are kept constant and are equal to about 0.2 and 0.3, respectively, in the $d=1.27$ cm and $d=1.91$ cm cases.

Measurements of Average and Local Mass Transfer

The top wall of the test channel consists of three rectangular slots into each of which a removable section of the top wall may be inserted (Fig. 1). To facilitate the measurements of the overall mass transfer coefficient and the distribution of the local mass transfer coefficient on the exposed surface of one of the primary walls between two blockages, two naphthalene cassettes are inserted into the slot between the two blockages in the top wall. Each cassette is constructed of aluminum and is about half as wide as the test channel. Each cassette has a 2.0-mm-deep cavity that is filled with naphthalene during a casting process. Once installed, the two cassettes rest side by side in the slot, on top of the two blockages and the test channel sidewalls, exposing a smooth, flat, naphthalene surface. During an experiment, mass is transferred from the naphthalene surfaces of the two cassettes to the air that flows through the test channel and the holes in the blockages, but all other surfaces exposed to the air are mass transfer inactive.

The two naphthalene cassettes are designed such that they can be quickly inserted into and removed from one of the three slots in the top wall. At the beginning and at the end of an experiment for determining the average mass transfer coefficient, the cassettes are weighed one at a time with a Sartorious electronic balance, which has a range of up to 160.0 g and a resolution of 0.1 mg.

To determine the distribution of the local mass transfer coefficient in an experiment, the elevations at a grid of 1100 points (50×22) on the naphthalene surface and on the top surface of the rim of each cassette are measured with a Starrette electronic depth gage at the beginning and at the end of the experiment. The depth gage has a lever type LVDT head, a range of ±0.2 mm, and a resolution of 0.002 mm. A Velmax NF90 controller, two stepper motors, a desktop computer, National Instruments data acquisition hardware, and a LABVIEW computer program are used to move the cassette on a coordinate table into position to facilitate the elevation measurements and to record the output from the electronic depth gage. The elevation measurements on the top surface of the rims of the cassette are needed to determine two reference planes of the naphthalene surface for calculating the elevation changes at the almost 1000 points on the naphthalene surface.

During an experiment, air is drawn into the test channel from the air-conditioned laboratory and exits the test apparatus to the outside of the building in which the laboratory is located. The temperature of the air is measured with two thermocouples and monitored with the computer controlled data acquisition system throughout the duration of the experiment. These thermocouples are calibrated with a constant temperature bath against a calibrated standard that is traceable to NIST. Also, before each experiment, the electronic depth gage or the electronic balance is calibrated with calibration standards that are supplied by the respective manufacturer.

To ensure the accuracy of the measured mass transfer data, each experiment is repeated multiple times. Supplementary experiments are conducted to check the calibration of the orifice flow meter (along with the manometers) and to determine the amounts of mass transfer during blower startup and shutdown for the experiments. The mass transfer corrections are needed because the duration of an experiment is defined as the period of time during which air flows steadily through the test channel.

Data Reduction

The overall and local mass transfer coefficients are defined, respectively, as

$$\bar{h}_m = \frac{\Delta M_n/\Delta t}{A_s(\rho_{v,w}-\bar{\rho}_{v,b})} \tag{1}$$

$$h_m = \frac{\dot{M}_n''}{\rho_{v,w}-\rho_{v,b}} = \frac{\rho_s \Delta z/\Delta t}{\rho_{v,w}-\rho_{v,b}} \tag{2}$$

where ΔM_n is the net mass transfer from a naphthalene surface to the air, $\dot{M}_n''$ is the local naphthalene mass flux, Δz is the local change of elevation on the naphthalene surface, Δt is the duration of the experiment, and ρ_s is the density of solid naphthalene. In the above equations, $\rho_{v,w}$ is the local vapor density of naphthalene at the wall and is evaluated using the ideal gas law, in which the vapor pressure is determined using the vapor pressure-temperature correlation for naphthalene by Ambrose et al. [16].

$$T_w \log(p_{v,w}) = \frac{a_0}{2} + \sum_{s=1}^{3} a_s E_s(x) \tag{3}$$

with

$$E_1(x) = x \quad E_2(x) = 2x^2 - 1 \quad \text{and } E_3(x) = 4x^3 - 3x \tag{4}$$

where $a_0=301.6247$, $a_1=791.4937$, $a_2=-8.2536$, $a_3=0.4043$, and $x=(2T_w-574)/114$.

The average bulk vapor density of naphthalene, $\bar{\rho}_{v,b}$, in Eq. (1) is the average of the bulk vapor densities at the upstream and downstream edges of the naphthalene surface and is calculated as

$$\bar{\rho}_{v,b} = \frac{1}{2}\left[\left(\frac{\dot{M}_n}{\dot{V}}\right)_{\text{upstream}} + \left(\frac{\dot{M}_n}{\dot{V}}\right)_{\text{downstream}}\right] \quad (5)$$

The bulk vapor density is equal to zero upstream of the naphthalene surface, because there is no naphthalene vapor in the air passing through the holes in the upstream blockage. The local bulk vapor density, $\rho_{v,b}$, in Eq. (2) for determining the local mass transfer coefficient at a point on the naphthalene surface is the rate of total mass transfer from the naphthalene surface upstream of the point divided by the air volumetric flow rate.

The average and local Sherwood numbers are defined, respectively, as

$$\overline{\text{Sh}} = \frac{\bar{h}_m D_h}{\sigma} \quad (6)$$

$$\text{Sh} = \frac{h_m D_h}{\sigma} \quad (7)$$

where σ is the mass diffusion coefficient for naphthalene vapor in the air. A correlation suggested by Goldstein and Cho [17] is used to determine the mass diffusion coefficient.

$$\sigma = 0.0681\left(\frac{T}{298.16}\right)^{1.93}\left(\frac{1.013 \times 10^5}{p}\right) \times 10^{-4} \quad (8)$$

According to the analogy between heat transfer and mass transfer described in Ref. [18],

$$\frac{\overline{\text{Nu}}}{\text{Nu}_0} = \frac{\overline{\text{Sh}}}{\text{Sh}_0} \quad (9)$$

$$\frac{\text{Nu}}{\text{Nu}_0} = \frac{\text{Sh}}{\text{Sh}_0} \quad (10)$$

where the reference Nusselt number and Sherwood number are based on the Dittus-Boelter correlation that is for a fully developed turbulent flow at the same Reynolds number through a smooth channel with the same hydraulic diameter as the test channel.

$$\text{Nu}_0 = 0.023\text{Re}^{0.8}\text{Pr}^{0.4} \quad (11)$$

$$\text{Sh}_0 = 0.023\text{Re}^{0.8}\text{Sc}^{0.4} \quad (12)$$

where Pr is the Prandtl number and Sc is the Schmidt number determined by

$$\text{Sc} = 2.28\left(\frac{T}{298.16}\right)^{-0.1526} \quad (13)$$

The Reynolds number for the airflow through the test section is

$$\text{Re} = \frac{4\dot{m}}{\mu P_w} = \frac{2\dot{m}}{\mu(W+H)} \quad (14)$$

where $\dot{m}$ is the mass flow rate of air, μ is the dynamic viscosity of air, P_w is the wetted perimeter of the test section, and W and H are the width and the height of the test section, respectively.

Based on the average pressure drop across two consecutive blockages, the friction factor is determined as

$$f = \frac{(\Delta p/\Delta x)D_h}{\rho \bar{u}^2/2} = 2\rho\left(\frac{\Delta p}{\Delta x}\right)D_h\left(\frac{A_c}{\dot{m}}\right)^2 \quad (15)$$

where Δx is the distance between pressure taps for measuring the pressure drops across two consecutive blockages, $\bar{u}$ is the average air velocity, and A_c is the cross-section area of the test channel. The friction factor is compared with a reference friction factor that is for fully developed turbulent flow in the channel with smooth walls.

$$f_0 = [0.79\ln(\text{Re}) - 1.64]^{-2} \quad (16)$$

The calculations of the uncertainty values of the Reynolds number, the Sherwood number, and the friction factor are based on a confidence level of 95%, uncertainty values of ±1.0% for all properties of the air, and ±0.5% for all physical dimensions [19]. Based on the maximum uncertainties for pressure at the orifice flow meter, the pressure drop across the orifice, and the Reynolds number for flow through the orifice flow meters of ±2.0%, ±3.9%, and ±2.4%, respectively, the maximum uncertainty of the air mass flow rate is calculated to be ±2.2%. The corresponding maximum uncertainty of the Reynolds number is ±2.5%.

Based on the uncertainty values of ±6.3% for ΔM_n, ±4.3% for $\rho_{v,w}$, and ±6.5% for $\rho_{v,b}$, the maximum uncertainty of the average mass transfer coefficient is found to be ±7.9%. Similarly, using uncertainty values of ±1.0% for ρ_s, ±9.5% for Δz, and ±0.1% for Δt, the maximum uncertainty of the local mass transfer coefficient is calculated to be ±10.4%. With the uncertainty value of ±2.0% for the diffusion coefficient of naphthalene vapor in air using the equation suggested by Goldstein and Cho [17], the estimated values of the maximum uncertainties for the average and local Sherwood numbers are ±8.2% and ±10.6%, respectively.

Using the maximum uncertainty values of ±6.8% for Δp and ±2.2% for $\dot{m}$, the maximum value of the uncertainty of the friction factor is estimated to be ±8.4%.

Presentation and Discussion of Results

According to the heat/mass transfer analogy [18], local and average heat transfer coefficients, and heat transfer enhancement, are related to, respectively, local and average mass transfer coefficients, and mass transfer enhancement, by $\text{Nu}/\text{Nu}_0 = \text{Sh}/\text{Sh}_0$ and $\overline{\text{Nu}}/\text{Nu}_0 = \overline{\text{Sh}}/\text{Sh}_0$ (Eqs. (9) and (10)). In this section, we will present local and average mass transfer results in terms of Sh/Sh_0 and $\overline{\text{Sh}}/\text{Sh}_0$, respectively, and it is understood that we may apply the presentation and discussion of these results to heat transfer, and replace Sh/Sh_0 and $\overline{\text{Sh}}/\text{Sh}_0$ by Nu/Nu_0 and $\overline{\text{Nu}}/\text{Nu}_0$ throughout.

Local Mass Transfer. In this study, the local mass transfer coefficient distributions on one of the two primary channel walls between two consecutive blockages were determined by measuring the changes of the elevations at a regular grid of 960 points (20×48) on the naphthalene surface of one of two cassettes during an experiment. Recall that the two naphthalene cassettes were installed side by side in a slot in the top channel wall between two blockages, exposing a smooth, flat, naphthalene surface to the airflow during an experiment. Local mass transfer results were obtained for eight different hole configurations, with aspect ratios between 1.0 and 3.36, and for two Reynolds numbers of 7000 and 17,000.

We will first discuss the variations of the local Sh/Sh_0 distribution downstream of the first, second, and third blockages, in the two cases of round holes and elongated holes with the largest aspect ratio of 3.36. We will then present the local Sh/Sh_0 distributions downstream of the second blockage only and examine the effect of the configuration of the holes on the local Sh/Sh_0 distribution. In subsequent sections, we will present the results on the effects of the hole configuration on the average mass transfer and the pressure drop.

Variation of Sh/Sh_0 *Downstream of Three Consecutive Blockages.* In Figs. 4 and 5, the local Sh/Sh_0 distributions downstream of the blockages are presented for the case of the smaller round holes (Case S-1) and in the case of the smaller elongated holes with the largest aspect ratio of 3.36 (Case S-4), respectively. In these figures, arrows indicate the direction of the main flow, which is from left to right, and the unshaded portions of the four blockages indicate the locations of the staggered holes. Also, only half of each of the Sh/Sh_0 distributions is shown—a broken line shows a symmetry plane.

In the case of the round holes (Case S-1, Fig. 4), there is a

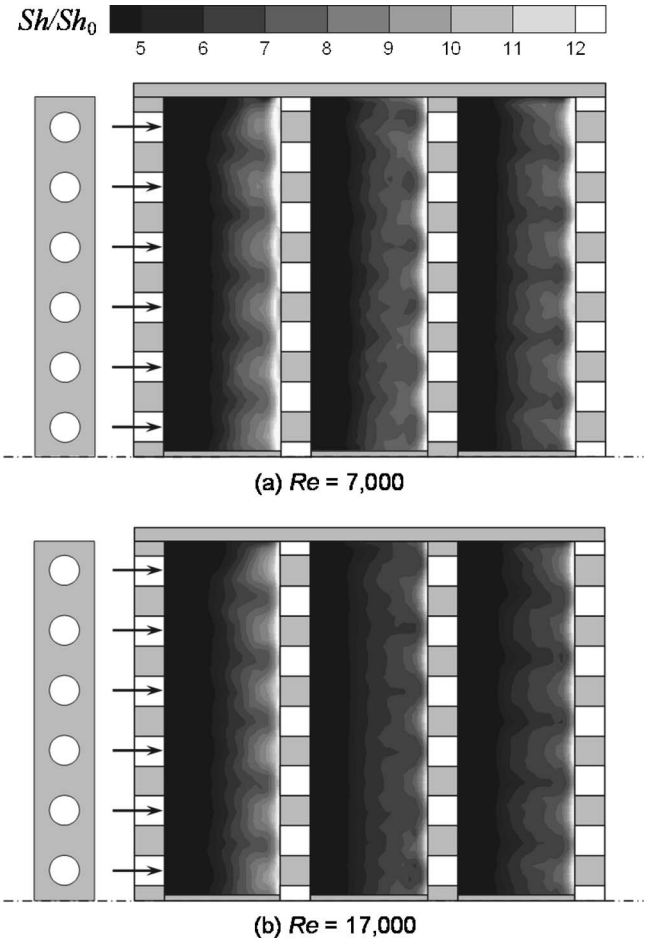

Fig. 4 Local mass transfer distributions on three wall segments downstream of blockages with the smaller round holes, Case S-1

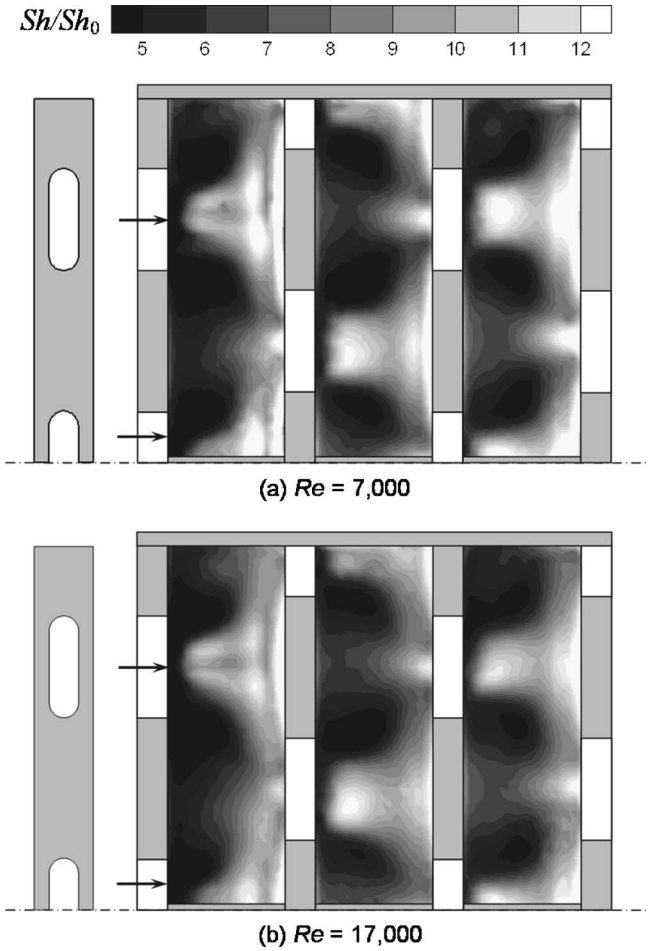

Fig. 5 Local mass transfer distributions on three wall segments downstream of blockages with the smaller elongated holes, Case S-4

monotonic increase of the Sh/Sh_0 value from less than 5.0 to over 12.0 between two blockages along the main flow direction. The local mass transfer is quite low immediately downstream of a blockage but is very high immediately upstream of a blockage. The spanwise variation of Sh/Sh_0 is much smaller than the streamwise variation. Immediately upstream of a blockage, the Sh/Sh_0 value is slightly lower at a hole than between two adjacent holes. The Sh/Sh_0 distributions on the three segments of the channel wall are quite similar, with Sh/Sh_0 values of 5.0 or less over 40–50% of each wall segment, and values of over 12 over only small discrete regions upstream of a blockage between two holes. Comparing Figs. 4(*a*) and 4(*b*), it appears that the blockages cause slightly higher Sh/Sh_0 distributions when Re=7000 than when Re=17,000.

After the air flows through the round holes in a blockage, a large portion of the jet impinges onto the upstream face of the downstream blockage, because the holes in consecutive blockages are staggered. There does not appear to be any reattachment of the air jets. The air is then deflected toward the two primary channel walls, causing the very high local mass transfer immediately upstream of the downstream blockage. The deflected airflow toward each channel wall may turn tangential to the wall before it is lifted from the wall and is forced to flow through the holes along the downstream blockage. A portion of the deflected airflow may turn upstream along the wall and is drawn into the recirculation zones with relatively slow moving flow between the air jets passing through the holes in the upstream blockage and the wall. The individual jets of air cause a periodic spanwise variation of the local mass transfer over each wall segment between consecutive blockages, although the spanwise variation is small compared with the streamwise variation between the blockages.

In the case of the elongated holes with an aspect ratio of 3.36 (Case S-4, Fig. 5), the spanwise variation of Sh/Sh_0 is quite large, although it is not as large as the streamwise variation. The local mass transfer is still very high immediately upstream of a blockage, with Sh/Sh_0 values of over 12.0. However, the local mass transfer is also quite high in an isolated region downstream of a hole, with Sh/Sh_0 values of over 12.0, while the values may be as low as less than 5.0 downstream of a blockage between two holes. The Sh/Sh_0 distribution downstream of the first blockage is slightly different than the similar distributions downstream of the second and third blockages. Comparing Figs. 5(*a*) and 5(*b*), while corresponding Sh/Sh_0 distributions are similar, the blockages with the elongated holes again cause slightly higher Sh/Sh_0 distributions when Re=7000 than when Re=17,000.

After the air flows through the wide opening of an elongated hole in a blockage, a portion of the flow impinges onto the upstream face of the downstream blockage between two staggered holes. The deflected airflow toward each channel wall again causes the high mass transfer immediately upstream of the downstream blockage between two holes. The local mass transfer distributions in Fig. 5 show that there is reattachment of the air jet on the channel wall, causing the isolated region of high mass transfer downstream of the hole. Also, the low mass transfer region that is sandwiched between two regions of even lower mass transfer regions (with Sh/Sh_0 values below 5.0), downstream of a blockage,

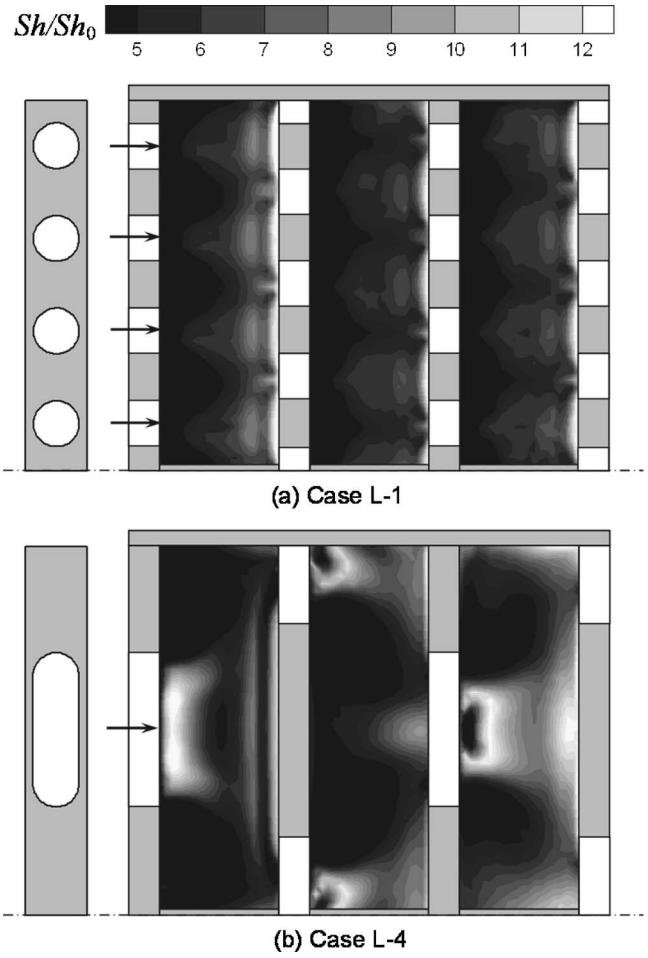

Fig. 6 Local mass transfer distributions on three wall segments downstream of blockages with the larger round and elongated holes, Re=7000

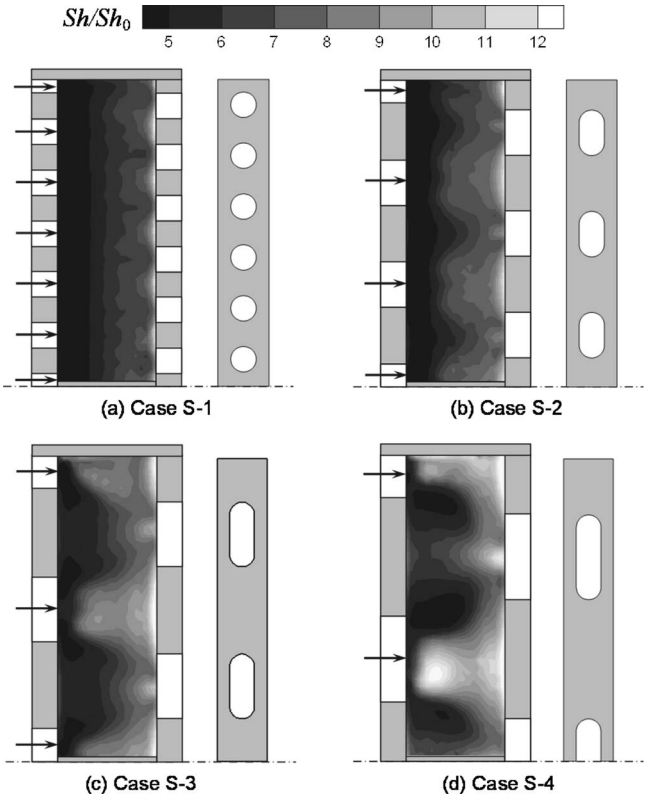

Fig. 7 Local mass transfer distributions on second wall segment downstream of second blockage with the smaller holes, Cases S-1–S-4, for Re=17,000

may indicate the existence of two counter-rotating vortices downstream of the blockage between two holes. The differences between the mass transfer distribution on the first wall segment and the similar mass transfer distributions on the two downstream wall segments may be the results of the airflow approaching the first blockage from an open wide channel while the airflow leaves an upstream blockage as individual jets before it approaches the second and third blockages. The effect of the entrance on the mass transfer distribution is more evident in Fig. 5 for Case S-4 with elongated holes than in Fig. 4 for Case S-1 with round holes.

In Figs. 6(*a*) and 6(*b*), the local Sh/Sh_0 distributions are presented for the cases of the larger round holes (Case L-1) and the larger holes with the largest aspect ratio of 3.36 (Case L-4), respectively, and for Re=7000. The Sh/Sh_0 distributions in Fig. 6(*a*) are similar to those in Fig. 4(*a*), except that the Sh/Sh_0 values are higher immediately downstream of the larger holes, resulting in larger periodic spanwise variations of the Sh/Sh_0 distributions in Case L-1 for the larger holes than in Case S-1 for the smaller holes. In Fig. 6(*a*), distinctive local high mass transfer regions upstream of a blockage indicate that there may be flow reattachment of the air jets from the holes along an upstream blockage. The Sh/Sh_0 values in these reattachment regions, however, are much smaller than those in the very high mass transfer region immediately upstream of a blockage resulting from the deflection of the jets off the upstream face of the blockage. Flow reattachment downstream of the large round holes is not as evident for Re=17,000 (Ahn [20]). These results are consistent with those for round holes obtained in an earlier study in Ref. [11].

In the case of the larger holes with the largest aspect ratio of 3.36 (Case L-4), there are only two holes along each blockage and there is a rather wide section of the blockage between two holes that does not allow the flow to pass. Figure 6(*b*) shows that the Sh/Sh_0 values are large downstream of the holes, where flow reattachment is clearly evident, and in a wide region upstream of a blockage between two holes, where the flow is deflected toward the channel wall. However, there are large regions of very low Sh/Sh_0 values downstream of the blockage between two holes and between a hole and the channel sidewall. Because of the geometry of the blockages in Case L-4, with two large "slots" separated from each other and from the sidewalls by very wide sections of the blockage, the spanwise variation of Sh/Sh_0 may be larger than the streamwise variation, and the Sh/Sh_0 distributions are different on the three wall segments between consecutive blockages. Figure 6(*b*) also shows that the Sh/Sh_0 distribution is the lowest on the first wall segment and the highest on the third and last wall segment.

Effect of Hole Configuration on Sh/Sh_0 *Distribution Downstream of Second Blockage*. To examine the effect of the hole aspect ratio on the local mass transfer distributions downstream of blockages with holes, the Sh/Sh_0 distributions on the second wall segment, between the second and third blockages, for the four cases with the smaller holes (Cases S-1–S-4) are presented in Fig. 7 for Re=17,000. In the case of the round holes, Fig. 7(*a*) again shows that the monotonic variation of Sh/Sh_0 in the main flow direction is much larger than the spanwise Sh/Sh_0 variation. It can be seen from Fig. 7 that increasing the hole aspect ratio increases the spanwise Sh/Sh_0 variation. Increasing the hole aspect ratio appears to increase the overall mass transfer on the wall segment, since there are larger regions of higher mass transfer in the larger hole aspect ratio cases. In Cases S-3 and S-4, there are regions with relatively high mass transfer downstream of the holes in the

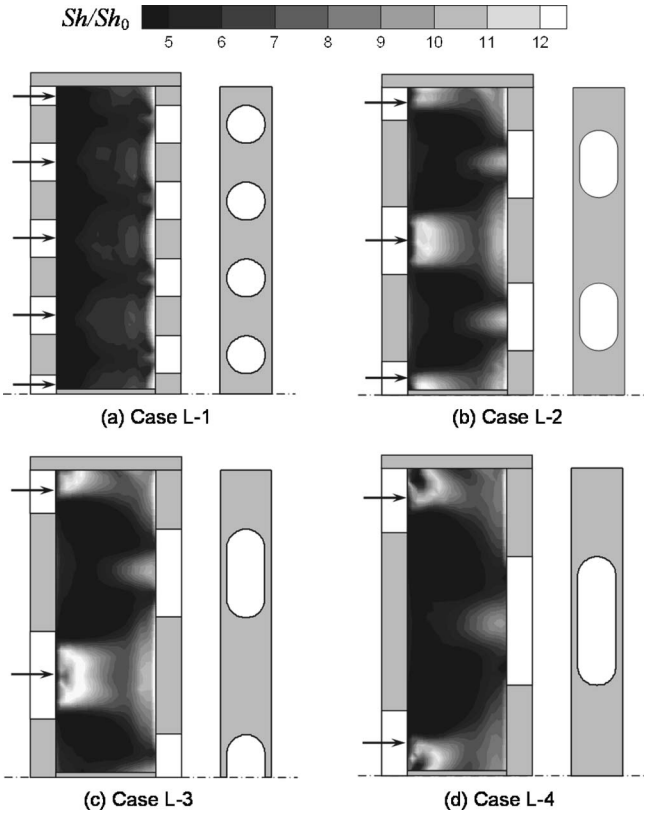

Fig. 8 Local mass transfer distributions on second wall segment downstream of second blockage with the larger holes, Cases L-1–L-4, for Re=17,000

second blockage. There are also regions with clearly very high mass transfer upstream of the third blockage between two holes, and the size of these regions increases with increasing hole aspect ratio.

For airflow through the smaller round holes in a blockage, a large portion of each jet either impinges onto the upstream face of the downstream blockage, and is then deflected toward the two primary channel walls, or passes straight through the two staggered holes in the downstream blockage. The deflection of the jet toward the walls causes the high local mass transfer immediately upstream of the downstream blockage.

For a given total hole-to-channel area ratio, increasing the aspect ratio of the holes reduces the number of holes and increases the distance between adjacent holes. The elongated holes with a larger aspect ratio cause a larger spanwise variation of the local mass transfer coefficient, with larger values immediately downstream of the holes in the upstream blockage but larger regions with small values of the local mass transfer coefficient downstream of the upstream blockage between adjacent holes. The larger values of the mass transfer coefficient downstream of the wider holes are the results of the shapes of the wider jets leaving the elongated holes, flow reattachment immediately downstream of the elongated holes, and the deflection of the wider jets toward the walls upstream of the downstream blockage. The mass transfer coefficient is small over larger regions downstream of the upstream blockage with the wider holes because there are larger counter-rotating vortices with relatively slow moving flow downstream of the wider section of the blockage where the flow is blocked.

The Sh/Sh_0 distributions on the second wall segment for the four cases with the larger holes (Cases L-1–L-4) are presented in Fig. 8 for Re=17,000. To maintain the same total hole-to-channel area ratio of 0.295 in these four cases, doubling the area of a round hole reduces the number of holes from 8 in Case L-1 to 4 in Case L-2. In Case L-3, for the holes with an aspect ratio of 2.57, there are only three holes in each blockage, while in Case L-4, for the holes with an aspect ratio of 3.36, there are only two holes in a blockage. These large elongated holes, or slots, are spaced rather far apart along the blockages. Figure 8 shows that the mass transfer is very low downstream of the wide sections of the upstream blockage between holes, and the size of the low Sh/Sh_0 regions increases with an increase of the distance separating the holes. As a result, for the three cases with larger elongated holes, the mass transfer distribution appears to be lower when the distance separating the holes is larger. It will be shown in the next section that the average mass transfer is lower in Case L-3 than in Case L-2 and is lower in Case L-4 than in Case L-3.

The flow reattaches on the channel wall downstream of the larger elongated holes in Cases L-2–L-4. The spanwise Sh/Sh_0 variation is larger in these three cases than in Case L-1 for the round holes, as a result of the large Sh/Sh_0 values in the regions of flow reattachment downstream of the elongated holes and upstream of the downstream blockage where the flow is deflected toward the channel wall, and the very low Sh/Sh_0 values downstream of the upstream blockage between the holes.

Based on the local mass transfer results presented in Figs. 7 and 8, the smaller elongated holes with the largest aspect ratio of 3.36 in Case S-4 appear to enhance the mass transfer the most. The mass transfer may be enhanced further by increasing the number of these holes in the blockages, since the mass transfer is quite high downstream of the holes and decreasing the spacing between two holes also reduces the size of the low mass transfer regions downstream of the blockages between two holes. Also, increasing the number of holes, which increases the hole-to-channel area ratio, should reduce the pressure drop across the blockages.

Average Mass Transfer. The average mass transfer on a wall segment was obtained both by weighing the two naphthalene cassettes, located side by side in a slot in the top channel wall between two blockages, before and after each experiment, and by determining the area-weighted average of the 960 local Sh/Sh_0 values, on the naphthalene surface of one of the two cassettes, that were measured in a separate experiment. For all of the experiments, the Sh/Sh_0 values obtained by weighing the two cassettes differed by less than 2.1% (the average of the variations was 0.4%, with a standard deviation of 1.1%), while the $\overline{Sh}/Sh_0$ values obtained by weighing the cassettes and by averaging the local Sh/Sh_0 values differed by not more than 4.9% (the average of the variations was 1.9% and the standard deviation was 2.2%). These variations were well within the estimated uncertainty value of 8.2% for $\overline{Sh}/Sh_0$.

In Ref. [20], supplementary heat transfer experiments were conducted to obtain the average heat transfer coefficients on three wall segments downstream of the same blockages in this study, using the test section of this study, three copper blocks as the wall segments between blockages, three flexible electric heaters to supply heat to the copper blocks, and small-gage thermocouples (seven in each copper block) to measure the wall and air temperatures, for the same two airflow rates. The effect of the hole configuration on $\overline{Nu}/Nu_0$ based on the heat transfer measurements was found to be consistent with the effect on $\overline{Sh}/Sh_0$ in this study. The $\overline{Nu}/Nu_0$ values in the heat transfer study were lower than corresponding $\overline{Sh}/Sh_0$ values in this study by not more than 9.9%. For all eight hole configurations studied, the heat transfer data were lower than the mass transfer data by 4.9% on average, with a standard deviation of 2.7%.

In Fig. 9, the average Sherwood number ratios on the three wall segments for Cases S-1, S-4, L-1, and L-4 are presented. These four cases are for round holes and elongated holes with the largest aspect ratio of 3.36. The corresponding local mass transfer distri-

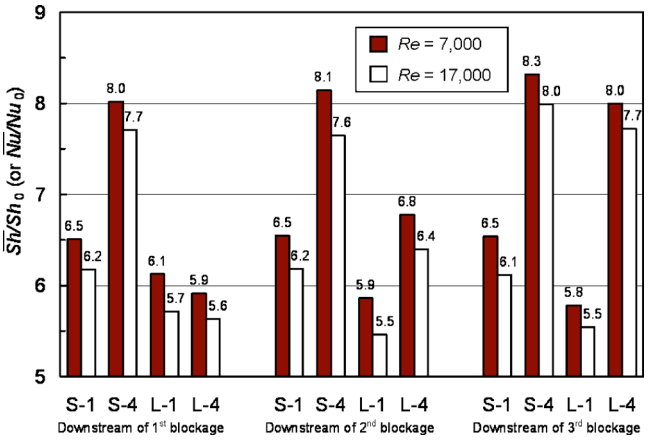

Fig. 9 Mass (heat) transfer enhancement on three wall segments between blockages with round holes and elongated holes with the largest aspect ratio

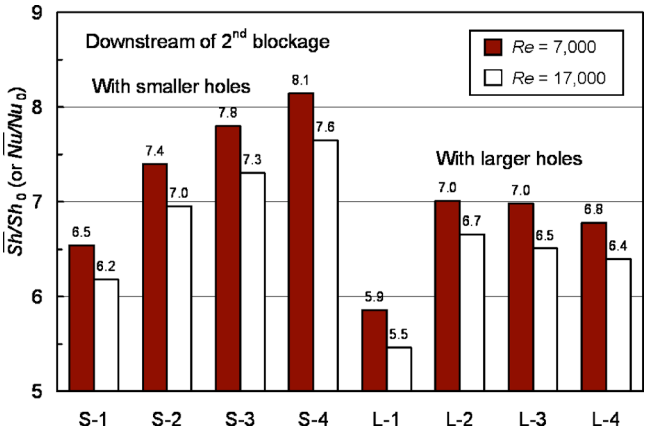

Fig. 10 Mass (heat) transfer enhancement on second wall segment between second and third blockages with round and elongated holes

butions for these cases have already been given in Figs. 4–6 and discussed earlier. Based on the results presented in Fig. 9, the following trends can be observed.

- In all cases, the average mass transfer enhancement is lower when the airflow rate is higher. The $\overline{Sh}/Sh_0$ value is lower when Re=17,000 than when Re=7000—by 3.5–6.8%.
- For the smaller holes, the average mass transfer is about the same on all three wall segments. In Case S-1, for the round holes, the $\overline{Sh}/Sh_0$ values on the three wall segments are within 1.1% of one another, with values of about 6.5 and 6.2, respectively, for Re=7000 and 17,000. In Case S-4, for the wide elongated holes, the $\overline{Sh}/Sh_0$ values on the two upstream wall segments are within 1.5% of each another but are slightly higher by 2.1–4.5% on the third wall segment. The $\overline{Sh}/Sh_0$ values are 25% and 26% higher in Case S-4 than in Case S-1, for Re=7000 and 17,000, respectively.
- For the larger round holes (Case L-1), the average mass transfer is the highest on the first wall segment and the lowest on the last wall segment, but the differences between the $\overline{Sh}/Sh_0$ values on the two wall segments are less than 5.6%. The $\overline{Sh}/Sh_0$ values of between 5.5 and 6.1 on the wall segments in this case (for the larger round holes) are lower than values of between 6.1 and 6.5 in Case S-1, for the smaller round holes.
- In Case L-4, there are only two large elongated holes along each blockage and it has been shown that the $\overline{Sh}/Sh_0$ distributions on the three wall segments were very different and that there were very large regions of low $\overline{Sh}/Sh_0$ values in the distribution on the first wall segment. Figure 9 shows that the $\overline{Sh}/Sh_0$ values are small on the first wall segment, but are 14–15% larger on the second wall segment, and are the highest on the last wall segment, with values of about 36% over those on the first wall segment.

In Fig. 10, the average Sherwood number ratios on the second wall segment for all hole configurations are compared. The figure shows that the average mass transfer on the second wall segment is higher in the four cases for the smaller holes than in the corresponding cases for the larger holes. Again, in all cases, the $\overline{Sh}/Sh_0$ value is lower when Re=17,000 than when Re=7,000—with a maximum difference of 6.8%. For the smaller holes, the average mass transfer increases as the aspect ratio of the holes is increased. The maximum $\overline{Sh}/Sh_0$ values for the widest holes (Case S-4) are about 24% higher than those for the round holes (Case S-1). The local Sh/Sh_0 distributions in Fig. 7 showed that there was significant mass transfer enhancement downstream of the wider holes, because of flow reattachment, and in regions upstream of the wide sections of the downstream blockage between staggered holes, as a result of the deflection of the flow from the downstream blockage toward the channel wall.

For the larger holes, the average mass transfer is again the lowest for the round holes (Case L-1) but is the highest for the elongated holes with an aspect ratio of 1.79 (Case L-2). With a further increase of the hole aspect ratio, the $\overline{Sh}/Sh_0$ value decreases. The increase of the size of the large low mass transfer regions downstream of the wide sections of a blockage between holes may contribute to the decrease of the average mass transfer with an increase of the aspect ratio of the larger holes (see Fig. 8).

Friction Factor. The pressure drops across the blockages were measured with five rows of static pressure taps, along with a calibrated pressure transducer with a digital readout. Three pressure taps were installed in a spanwise row in the bottom wall at a distance of 2.54 cm (half the distance between the blockages) upstream of the first blockage. Nine pressure taps were installed in three rows in the bottom channel wall halfway between the consecutive blockages. Three additional pressure taps were located at a distance of 2.54 cm downstream of the last blockage (see Fig. 2). The friction factor that is to be reported here was calculated based on the average of the three pressure drops across two consecutive blockages—between the pressure taps in the first and third rows, the second and fourth rows, and third and fifth rows.

As expected, with the flow cross section reduced by about 70% and 80% by the blockages with holes of two sizes in this study, the pressure drops across the blockages are much larger than the pressure drop for airflow through an open rectangular channel at the same flow rate. Figure 11 shows that the smaller holes in Cases S-1–S-4 cause larger pressure drops than the larger holes in Cases L-1–L-4. The friction factor ratio, f/f_0, increases as the hole aspect ratio is increased, with values ranging from 780 to 1810 for the blockages with the smaller holes and from 330 to 1030 for the blockages with the larger holes, although the hole-to-channel area ratio is the same (and equal to 0.196) in all four cases with the smaller round and elongated holes and in the four cases with the larger holes (equal to 0.295). The wider sections of the blockages between staggered holes with a larger aspect ratio appear to increase the resistance to the airflow through the channel more than the blockages that have more holes with a smaller aspect ratio and a smaller spacing between holes.

In all cases, the friction factor ratio, f/f_0, is larger when Re =17,000 than when Re=7000.

Thermal Performance. The thermal performance was evaluated based on the average mass (heat) transfer enhancement on the

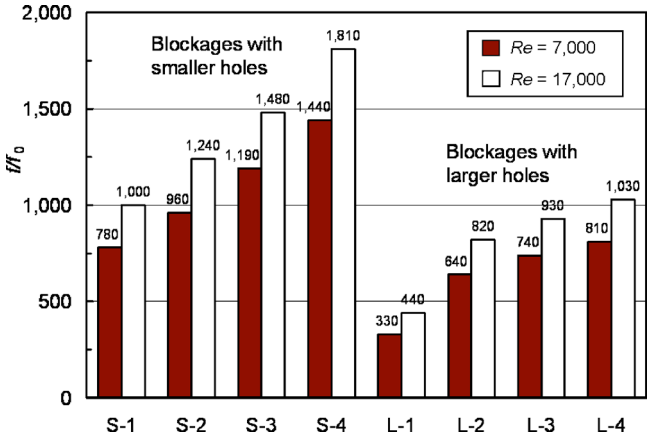

Fig. 11 Pressure drop across two consecutive blockages with round and elongated holes

wall segment between the second and third blockages and pressure drop across the second and third blockages. Although the smaller holes enhance more mass (heat) transfer than the larger holes, they also cause a larger increase of the pressure drop than the larger holes. While $\overline{\mathrm{Sh}}/\mathrm{Sh}_0$ ($\overline{\mathrm{Nu}}/\mathrm{Nu}_0$) decreases with increasing Re, f/f_0 increases (see Figs. 10 and 11). Figure 12 compares the thermal performances of the blockages with the smaller and the larger holes. In all cases, the thermal performance (TP) value decreases with an increase of the Reynolds number. The blockages with the larger holes outperform those with the smaller holes slightly, with TP values ranging from 0.63 to 0.85 versus values from 0.62 to 0.75. For the blockages with the smaller holes, the TP values for the three elongated hole cases are about the same and are slightly higher than those for the round hole case. For the blockages with the larger holes, the TP decreases with an increase of the hole aspect ratio while keeping the total hole-to-channel cross-sectional area ratio constant.

Concluding Remarks

Naphthalene sublimation experiments were conducted to study mass (heat) transfer enhancement by blockages with round and elongated holes in a wide rectangular channel that modeled the cooling channel in the trailing edge region of an internally cooled gas turbine blade. Local and average mass (heat) transfer results were obtained for eight configurations of staggered holes with two sizes and four aspect ratios in the blockages and for two Reynolds numbers. For the conditions under which the experiments were conducted and the geometries of blockages and the test sections that were studied, the results are summarized as follows.

- The distribution of the local mass (heat) transfer is very much dependent on the configuration of the holes in the blockages. For the blockages with round holes in this study, the mass (heat) transfer on the wall segment between two blockages is low downstream of the upstream blockage and is high upstream of the downstream blockage, with much larger streamwise variation than spanwise variation. For the blockages with elongated holes in this study, the mass (heat) transfer is high downstream of the holes, as a result of flow reattachment, but is very low downstream of the wide section of the blockage between holes, and the spanwise variation of the local mass (heat) transfer may be as large as the streamwise variation. The local mass (heat) transfer distribution is not significantly affected by changing the airflow rate.
- Blockages with holes may cause the average mass (heat) transfer on the wall segments between two blockages in a channel to be much higher than that for a fully developed flow through an open channel with no blockages at the same flow rate, but they also significantly increase the pressure drop. The blockages with round and elongated holes in this study increase the average mass (heat) transfer by 4.5–7.3 times over the corresponding fully developed channel flow value. The blockages with the smaller holes enhance the average mass (heat) transfer more than those with the larger holes, but also increase the pressure drop more than the blockages with the larger holes, by as much as 136%, for the same hole aspect ratio.

Based on the results of this study, blockages with elongated holes and a small spacing between holes are recommended for a cooling channel near the trailing edge of an internally cooled gas turbine airfoil. Additional parametric studies are needed to obtain local and average heat transfer data to optimize the size and the aspect ratio of the holes in the blockages, the spacing between the holes, and the spacing between two blockages, relative to the channel height. Heat transfer data are also needed on the upstream surfaces of the blockages and on the surfaces of the holes, where the heat transfer is expected to be very high, and also on the downstream surfaces of the blockages since a substantial amount of heat may be conducted from the pressure and suction walls to the blockages and is then transferred from these surfaces to the air in a cooling channel near the trailing edge of an airfoil. The total area of the surfaces of the blockages may be comparable with the area of the surfaces of the pressure and suction walls that are exposed to the cooling air.

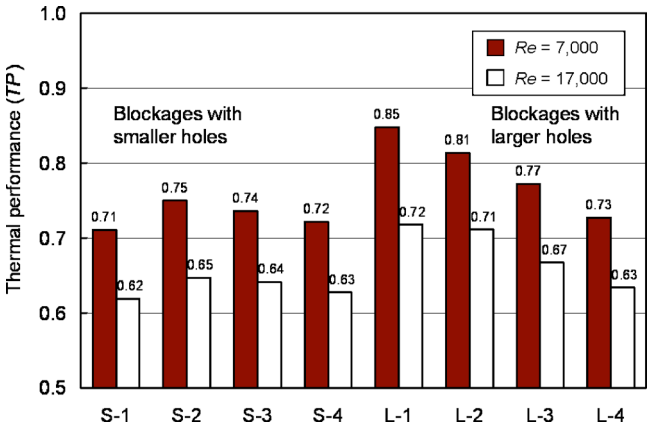

Fig. 12 Thermal performance based on mass transfer enhancement downstream of second blockage and pressure drop across two consecutive blockages

Nomenclature

a = width of round or elongated holes in blockages, m
A_c = flow cross-sectional area of test channel, m^2
A_s = surface area, m^2
b = center-to-center spacing between adjacent holes in blockages, m
d = diameter of holes in blockages, m
D_h = hydraulic diameter of test channel, m
f = friction factor based on pressure drop across two consecutive blockages and distance between pressure taps
f_0 = reference friction factor for fully developed turbulent flow in smooth channel
h_m = local mass transfer coefficient, m/s
$\bar{h}_m$ = average mass transfer coefficient, m/s
H = height of test channel
$\dot{m}$ = air mass flow rate, kg/s

$\dot{M}_n$ = rate of total mass transfer from upstream naphthalene surface, kg/s
$\dot{M}''_n$ = local naphthalene mass flux, $kg/(m^2\,s)$
$\underline{Nu}$ = local Nusselt number
$\overline{Nu}$ = average Nusselt number
Nu_0 = reference Nusselt number for fully developed turbulent flow in smooth channel
p = pressure, N/m^2
$p_{v,w}$ = vapor pressure on naphthalene surface, N/m^2
P_w = perimeter of test channel, m
Re = Reynolds number
Sc = Schmidt number
$\underline{Sh}$ = local Sherwood number
$\overline{Sh}$ = average Sherwood number
Sh_0 = reference Sherwood number for fully developed turbulent flow in smooth channel
T = temperature, K
T_w = wall temperature, K
TP = thermal performance, defined as $(\overline{Nu}/Nu_0)/(f/f_0)^{1/3}$
$\bar{u}$ = average velocity, m/s
$\dot{V}$ = volumetric flow rate of air, m^3/s
W = width of the test channel, m

Greek Symbols

ΔM_n = total mass transfer from naphthalene surface to air, kg
Δp = pressure drop across two consecutive blockages, N/m^2
Δt = duration of experiment, s
Δx = distance between two pressure taps for measuring pressure drop across two blockages, m
Δz = local change of elevation on naphthalene surface, m
μ = dynamic viscosity of air, $N\,s/m^2$
ρ = density of air, kg/m^3
$\rho_{v,b}$ = local bulk vapor density of naphthalene, kg/m^3
$\bar{\rho}_{v,b}$ = average bulk vapor density of naphthalene, kg/m^3
ρ_s = density of solid naphthalene, kg/m^3
$\rho_{v,w}$ = vapor density of naphthalene on naphthalene surface, kg/m^3
σ = mass diffusion coefficient of naphthalene vapor in air, m^2/s

References

[1] Han, J. C., Dutta, S., and Ekkad, S. V., 2000, *Gas Turbine Heat Transfer and Cooling Technology*, Taylor & Francis, New York, pp. 251–529.
[2] Park, C. W., Yoon, C., and Lau, S. C., 2000, "Local Heat (Mass) Transfer in a Diagonally-Oriented Rotating Two-Pass Channel With Rib-Roughened Walls," ASME J. Heat Transfer, **122**(1), pp. 208–211.
[3] Taslim, M. E., Pan, Y., and Bakhtari, K., 2000, "Experimental Racetrack Shaped Jet Impingement on a Roughened Leading-Edge Wall With Film Holes," ASME Paper No. GT-2002–30477.
[4] Ligrani, P. M., and Mahmood, G. I., 2003, "Spatially Resolved Heat Transfer and Friction Factors in a Rectangular Channel With 45 Deg Angled Crossed-Rib Turbulators" ASME J. Turbomach., **125**, pp. 575–584.
[5] Wright, L. M., Lee, E., and Han, J. C., 2003, "Influence of Entrance Geometry on Heat Transfer in Narrow Rectangular Cooling Channels (AR=4:1) With Angled Ribs," ASME Paper No. IMECE2003-42572.
[6] Tafti, D., 2003, "Large-Eddy Simulations of Heat Transfer in a Ribbed Channel for Internal Cooling of Turbine Blades," ASME Paper No. CT2003-38122.
[7] Acharya, S., Agarwal, P., and Nikitopoulos, D. E., 2004, "Heat/Mass Transfer in a 4:1 AR Smooth and Ribbed Coolant Passage With Rotation at 90-degree and 45-degree Orientations," ASME Paper No. GT2004–53928.
[8] Lee, D. H., Rhee, D.-H., and Cho, H. H., 2006, "Heat Transfer Measurements in a Rotating Equilateral Triangular Channel With Various Rib Arrangements," ASME Paper No. GT-2006–90973.
[9] Lau, S. C., Cervantes, J., Han, J. C., and Rudolph, R. J., 2006, "Internal Cooling Near Trailing Edge of a Gas Turbine Airfoil With Cooling Airflow Through Blockages With Holes," ASME Paper No. GT2006–91230.
[10] Moon, S. W., and Lau, S. C., 2003, "Heat Transfer Between Blockages With Holes in a Rectangular Channel," ASME J. Heat Transfer, **125**, 587–594.
[11] Lau, S. C., Cervantes, J., Han, J. C., Rudolph, R. J., and Flannery, K., 2003, "Measurements of Wall Heat (Mass) Transfer for Flow Through Blockages With Round and Square Holes in a Wide Rectangular Channel," Int. J. Heat Mass Transfer, **46**, pp. 3991–4001.
[12] Kukreja, R. T., and Lau, S. C., 1998, "Distributions of Local Heat Transfer Coefficient on Surfaces With Solid and Perforated Ribs," J. Enhanced Heat Transfer **5**(1), pp. 9–21.
[13] Hwang, J. J., Lia, T. Y., and Liou, T. M., 1998, "Effect of Fence Thickness on Pressure Drop and Heat Transfer in a Perforated-Fenced Channel," Int. J. Heat Mass Transfer **41** (4–5), pp. 811–816.
[14] Liou, T. M., and Chen, S. H., 1998, "Turbulent Heat and Fluid Flow in a Passage Distributed by Detached Perforated Ribs of Different Heights," Int. J. Heat Mass Transfer **41**(12), pp. 1795–1806.
[15] Buchlin, J. M., 2002, "Convective Heat Transfer in a Channel With Perforated Ribs," Int. J. Therm. Sci. **41**, pp. 332–340.
[16] Ambrose, D., Lawrenson, I. J., and Sprake, C. H. S., 1975, "The Vapor Pressure of Naphthalene," J. Chem. Thermodyn. **7**, pp. 1172–1176.
[17] Goldstein, R. J., and Cho, H. H., 1995, "A Review of Mass Transfer Measurements Using Naphthalene Sublimation," Exp. Therm. Fluid Sci. **10**, pp. 416–434.
[18] Eckert, E. R. G., 1976, "Analogies to Heat Transfer Processes," in *Measurements in Heat Transfer*, E. R. G. Eckert, and R. J. Goldstein, eds., Hemisphere, New York, pp. 397–423.
[19] Coleman, H. W., and Steele, W. G., 1889, *Experimentation and Uncertainty Analysis for Engineers*, Wiley, New York.
[20] Ahn, H. S., 2006, "Heat and Mass Transfer Enhancement for Flow Through Blockages With Round and Elongated Holes in a Rectangular Channel," Ph.D. thesis, Texas A&M University, College Station, TX.